Physica A 538 (2020) 122826

Contents lists available at ScienceDirect

Physica A

journal homepage: www.elsevier.com/locate/physa

Free convection flow and heat transfer of nanofluids in a cavity with conjugate solid triangular blocks: Employing Buongiorno's mathematical model

S.M. Hashem Zadeh [a], M. Sabour [b], S. Sazgara [c], M. Ghalambaz [d,e,*]

[a] Department of Mechanical Engineering, Shahid Chamran University of Ahvaz, Ahvaz, Iran
[b] Young Researchers and Elite Club, Ahvaz Branch, Islamic Azad University, Ahvaz, Iran
[c] Department of Mechanical Engineering, Dezful Branch, Islamic Azad University, Dezful, Iran
[d] Department for Management of Science and Technology Development, Ton Duc Thang University, Ho Chi Minh City, Vietnam
[e] Faculty of Applied Sciences, Ton Duc Thang University, Ho Chi Minh City, Vietnam

ARTICLE INFO

Article history:
Received 17 May 2019
Received in revised form 28 August 2019
Available online 24 September 2019

Keywords:
Conjugate natural convection
Buongiorno's model
Thermal conductivity parameter
Dynamic viscosity parameter

ABSTRACT

This study aims to investigate the conjugate natural convection heat transfer of nanofluids in a square enclosure with two solid triangular walls. The left and right walls of the cavity are held at a constant temperature of T_h and T_c, respectively, whereas the bottom and top are insulated. To assess the nanoparticles distribution inside the cavity that induced from the thermophoresis and Brownian motion, the Buongiorno's model was used. The governing nonlinear equations were solved in a non-uniform unstructured grid by employing the Galerkin finite element method. The governing parameters are Rayleigh number ($10^3 \le Ra \le 10^4$), thermal conductivity ratio of solid walls to the fluid ($1 \le R_k \le 500$), thermal conductivity parameter ($3 \le Nc \le 15$), thermal viscosity parameter ($3 \le Nv \le 15$), Brownian motion parameter ($5\times10^{-7} \le N_b \le 5\times10^{-6}$), Thermophoresis parameter ($10^{-7} \le N_b \le 10^{-6}$), thickness of the triangular walls ($0.1 \le m \le 0.75$) and the position of the blocks (normal or reverse position). The numerical results are reported as contours of isotherms, streamlines, heatlines and isoconcentrations and the local and average Nusselt numbers. The results show that the presence of the triangular blocks boosts the overall rate of heat transfer. The average Nusselt number increases as the R_k decreases. The overall rate of heat transfer decreases when the triangular walls are placed in the reverse position.

1. Introduction

Between all types of convection heat transfer, the natural convection, due to temperature or concentration gradient, is the most important heat transfer procedure where external power is not required. Enormous researchers studied the natural convection due to a large number of engineering applications such as the formation of microstructures during the cooling of molten metals, and fluid flows around shrouded heat-dissipation fins and solar ponds. Industrial applications of the free convection vary from air-cooling of computer chips in small scales to large scale process equipment [1].

The natural convection in the enclosures utilizing the partitions is an interesting issue for many studies [2]. According to the principle, the presence of partitions has substantial effects on the flow field, and as a result, it improves the

* Corresponding author.
E-mail addresses: mohsen.hashemzadeh@gmail.com (S.M.H. Zadeh), mohammad.ghalambaz@tdtu.edu.vn (M. Ghalambaz).

https://doi.org/10.1016/j.physa.2019.122826
0378-4371/

Nomenclature

C	Volume fraction of nanofluid
c_p	specific heat capacity (J/kg ^oK)
D_B	Brownian motion coefficient (m^2/s)
D_T	Thermophoresis coefficient (m^2/s)
G	Gravity (m/s^2)
H	Height of cavity (m)
H_1	Height of partition (m)
H	Heat functions
K	Thermal conductivity (W/m ^oK)
Le	Lewis number
L_1	Distance of vertical wall (m)
N_b	Brownian motion parameter
Nc	Thermal conductivity parameter
Nr	Buoyancy ratio
N_t	Thermophoresis parameter
Nu	Average Nusselt number
Nu_x	Local Nusselt number
Nv	Thermal viscosity parameter
m	Size of triangular (m)
P	Pressure (atm)
Pr	Prandtl number
Ra	Rayleigh number
R_c	Effective heat capacity ratio
R_k	Thermal conductivity ratio
T	Temperature (^oK)
U	velocity component in horizontal direction (m/s)
V	velocity component in vertical direction (m/s)
X	Cartesian coordinate in horizontal direction (m)
Y	Cartesian coordinate in vertical direction (m)

Greek symbols

α	Thermal diffusivity (m^2/s)
β	Thermal expansion coefficient (1/^oK)
θ	Non-dimensional temperature
$-$	Dynamic viscosity (Kg/m s)
ρ	Density (Kg/m^3)
φ	Normalized volume fraction of nanoparticles
ν	Kinematic viscosity (m^2/s)
γ	Penalty Parameter

Subscript

bf	Base fluid
C	Cold
H	Hot
nf	Nanofluid
P	Particles
S	Solid
0	initial value

Superscript

*	Dimensional quantity

overall thermal performance of the enclosures. An important role that the partitions can play in the enclosures is as thermal diodes. They can have various thermal performances in different directions, depending on the thermal boundary conditions and characteristics of the partitions [2]. In the literature, there are numerous studies about the natural convection heat transfer in the partitioned enclosures for various simple geometries, including square [3], triangular [4], rectangular [5] enclosures. Recently, the natural convection in complex geometries, including enclosures with partitions and conjugate heat transfer, has attracted the attention of researchers. Costa [6] has numerically investigated the natural convection in the partitioned square enclosure, including partitions (fixed two partitions on the top and bottom walls) filled with air. Costa [6] has analyzed the overall thermal performance through the Nusselt number. Kandaswamy et al. [7] performed a numerical study on the effect of baffle-cavity ratios on the buoyancy convection. Based on their study [7], the overall heat transfer in the cavity is increased for higher values of baffle-cavity.

Furthermore, Wu and Ching [8] experimentally investigated the laminar natural convection in the square cavity filled with air using aluminum partitions fixed on the top wall. In the study of Wu and Ching [8], the partitions have been attached in four places of the top wall with different sizes. As an important result, they [8] concluded that the presence of the partitions results in changes in flow and temperature fields of the fluid.

A wide range of industrial processes involves heat energy transfer. Heat transfer is an essential part of most of the industrial equipment. Thus, the enhancement of heating or cooling in these industrial processes could be extremely beneficial as it can save energy and decrease the overall costs. A novel fluid with unique properties called nanofluids has been introduced for almost two decades [3,9–16]. The Nanofluid is a new kind of heat transfer medium containing nanoparticles (1–100 nm) which are uniformly and stably distributed in a base fluid. These distributed nanoparticles, which are generally a metal or metal-oxide, greatly enhance the thermal conductivity of the nanofluid and increase conduction and convection coefficients and also allow more heat transfer [9].

In some of the recent studies, the investigation of natural convective heat transfer of nanofluids flow in enclosures has been performed [17–27]. For example, Oztop and Abu-Nada [28] investigated the heat transfer and fluid flow of natural convection in partially rectangular enclosures filled with nanofluids. They [28] found the increase of mean Nusselt number with boosting the nanoparticle volume fraction for whole values of Rayleigh number. Abu-Nada and Chamkha [29] have examined the effect of the CuO–EG–Water nanofluid properties on natural convection flow in enclosures using different thermal conductivity and variable viscosity models. In another work, they [30] have numerically studied the mixed convection flow of the water–Al_2O_3 nanofluid in a square enclosure. In their study [30], it is found that the presence of nanoparticles can substantially enhance the heat transfer. Moreover, Abu-Nada et al. [29] studied the effect of variable properties of the Al_2O_3-water and CuO–water nanofluids on the natural convection in enclosures and showed that CuO–water nanofluids cause a continuous decrease in Nusselt number with the increase of the volume fraction of nanoparticles at high Rayleigh numbers. Besides, a numerical study on the free convection in a square enclosure with curve boundaries filled with the Cu–water nanofluid has performed by Sheikholeslami et al. [31].

The present study aims to model and analysis the conjugate natural convection flow and heat transfer of nanofluids by considering the concentration distribution of nanoparticles in the enclosure. The conjugate heat transfer consists of two metallic enhancers. The heatlines, as suggested by Bejan [2], are utilized to demonstrate the flow of heat in the nanofluid and conjugate parts of the cavity. The conjugate enhancers, in the present work, do not play a role of the internal heater or cooler, but they have a significant effect on the local concentration of nanoparticles and the heat transfer process. To accomplish a realistic study, a substantial length, finite thickness, and thermal conductivity of the conjugate parts are considered as design parameters. The governing equations are transformed in a non-dimensional form and solved numerically using the finite element method. Finally, a case study has been accomplished for Kerosene–AL_2O_3 nanofluid. The present study aims to answer the following questions: What is the effect of the conjugate blocks on the local Nusselt number? What is the effect of conjugate blocks on the distribution of nanoparticles in the enclosure? Do conjugate blocks (the metallic part of the cavity) improve the heat transfer of nanofluids? With these questions in mind, a model of nanofluid for the conjugate heat transfer in an enclosure is introduced in the next section.

2. Geometric and mathematical models

2.1. Physics of the problem

A two-dimensional steady conjugate natural convection heat transfer of the nanofluids in the $L\times L$ square enclosure with two solid triangular walls is considered. The two solid walls are fixed on the top-right corner and bottom-left corner with triangular yield t^*. The Cartesian coordinate is considered and located at the center of the physical model. A schematic of the physical model is represented in Fig. 1. It is assumed that the temperatures of the left and right walls are T_h and T_c respectively, where $T_h > T_c$. The bottom and top walls are insulated. The enclosure walls are considered to be rigid,

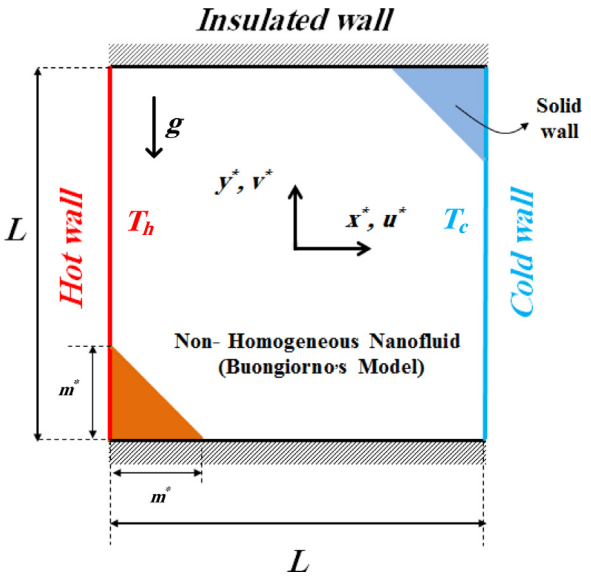

Fig. 1. Schematic diagram of the physical model.

conducting, and impermeable. Besides, the partitions are considered to be heat conductive. The nanofluid flow is assumed to be laminar and incompressible. The local physical properties of the nanofluid are to be constant. Moreover, Boussinesq's approximation is adopted.

2.2. Governing equations

Taking into account that the nanofluids are a dilute suspension of nanoparticles, the steady form of governing equations for mass, momentum and thermal energy, and the conservation for nanoparticles are represented here in dimensional Cartesian coordinates x^*, y^*as follow [32] and [33]:

$$\frac{\partial u^*}{\partial x^*} + \frac{\partial v^*}{\partial y^*} = 0 \tag{1}$$

$$\rho_{nf}\left(u^*\frac{\partial v^*}{\partial x^*} + v^*\frac{\partial v^*}{\partial y^*}\right) = -\frac{\partial \mathrm{p}^*}{\partial x^*} + \mu_{nf}\left(\frac{\partial^2 u^*}{\partial x^{*2}} + \frac{\partial^2 u^*}{\partial y^{*2}}\right) \tag{2}$$

$$\rho_{nf}\left(u^*\frac{\partial v^*}{\partial x^*} + v^*\frac{\partial v^*}{\partial y^*}\right) = -\frac{\partial \mathrm{p}^*}{\partial y^*} + \mu_{nf}\left(\frac{\partial^2 v^*}{\partial x^{*2}} + \frac{\partial^2 v^*}{\partial y^{*2}}\right) + \left\{\rho_p C + (1-C)\left[\rho_{bf}\left(1-\beta\left(T-T_c\right)\right)\right]\right\} g \tag{3}$$

$$\begin{aligned}&(\rho c)_{nf}\left(u^*\tfrac{\partial T}{\partial x^*} + v^*\tfrac{\partial T}{\partial y^*}\right) = \tfrac{\partial}{\partial x^*}\left(k_{nf}\tfrac{\partial T}{\partial x^*}\right) + \tfrac{\partial}{\partial y^*}\left(k_{nf}\tfrac{\partial T}{\partial y^*}\right)\\ &+ \left(\rho c_p\right)_p\left[D_B\left(\tfrac{\partial T}{\partial x^*}\tfrac{\partial C}{\partial x^*} + \tfrac{\partial C}{\partial y^*}\tfrac{\partial T}{\partial y^*}\right) + \tfrac{D_T}{T_c}\left(\left(\tfrac{\partial T}{\partial x^*}\right)^2 + \left(\tfrac{\partial T}{\partial y^*}\right)^2\right)\right]\end{aligned} \tag{4}$$

$$\left(u^*\frac{\partial C}{\partial x^*} + v^*\frac{\partial C}{\partial y^*}\right) = D_B\left(\frac{\partial^2 C}{\partial x^{*2}} + \frac{\partial^2 C}{\partial y^{*2}}\right) + \frac{D_T}{T_c}\left(\frac{\partial^2 T}{\partial x^{*2}} + \frac{\partial^2 T}{\partial y^{*2}}\right) \tag{5}$$

In addition, the heat conduction equation for the temperature in wall partitions which are mounted on the top and bottom walls is introduced as [6,15] and [34]:

$$\frac{\partial^2 T}{\partial x^{*2}} + \frac{\partial^2 T}{\partial y^{*2}} = 0 \tag{6}$$

where $R_k = k_s/k_{bf}$. The three sets of dimensional boundary conditions corresponding to the velocity, temperature, and nanoparticles concentration for Eqs. (1)–(6) are represented, respectively as:

$$u^* = v^* = 0 on\ the\ solid\ walls \tag{7a}$$

$$\begin{aligned}&T\left(-\tfrac{L}{2}, y^*\right) = T_h,\ T\left(\tfrac{L}{2}, y^*\right) = T_c\\ &\tfrac{\partial T}{\partial y^*}\Big|_{\left(x^*, -\frac{L}{2}\right)} = 0,\ \tfrac{\partial T}{\partial y^*}\Big|_{\left(x^*, \frac{L}{2}\right)} = 0.\end{aligned} \tag{7b}$$

$$\begin{aligned}
&\frac{\partial C}{\partial y^*}\Big|_{\left(-\frac{L}{2}+m^*\le x^*\le\frac{L}{2},-\frac{L}{2}\right)}=0,\ \frac{\partial C}{\partial y^*}\Big|_{\left(-\frac{L}{2}\le x^*\le\frac{L}{2}-m^*,\frac{L}{2}\right)}=0,\\
&D_B\ \frac{\partial C}{\partial x^*}\Big|_{\left(-\frac{L}{2},-\frac{L}{2}+m^*\le y^*\le\frac{L}{2}\right)}+\frac{D_T}{T_c}\ \frac{\partial T}{\partial x^*}\Big|_{\left(-\frac{L}{2},-\frac{L}{2}+m^*\le y^*\le\frac{L}{2}\right)}=0,\\
&D_B\ \frac{\partial C}{\partial x^*}\Big|_{\left(\frac{L}{2},-\frac{L}{2}\le y^*\le\frac{L}{2}-m^*\right)}+\frac{D_T}{T_c}\ \frac{\partial T}{\partial x^*}\Big|_{\left(\frac{L}{2},-\frac{L}{2}\le y^*\le\frac{L}{2}-m^*\right)}=0.\\
&D_B\ \frac{\partial C}{\partial n^*}\Big|_{\left(-\frac{L}{2}\le x^*\le-\frac{L}{2}+m^*,-(x^*+L)+m^*\right)}+\frac{D_T}{T_c}\ \frac{\partial T}{\partial n^*}\Big|_{\left(-\frac{L}{2}\le x^*\le-\frac{L}{2}+m^*,-(x^*+L)+m^*\right)}=0,\\
&D_B\ \frac{\partial C}{\partial n^*}\Big|_{\left(\frac{L}{2}-m^*\le x^*\le\frac{L}{2},-(x^*+m^*)+L\right)}+\frac{D_T}{T_c}\ \frac{\partial T}{\partial n^*}\Big|_{\left(\frac{L}{2}-m^*\le x^*\le\frac{L}{2},-(x^*+m^*)+L\right)}=0.
\end{aligned}\tag{7c}$$

and the boundary conditions on the interfaces (dimensionally) are introduced as:

$$\begin{aligned}
&T\left(-\frac{L}{2}\le x^*\le-\frac{L}{2}+m^*,-\left(x^*+L\right)+m^*\right)=T_s\left(-\frac{L}{2}\le x^*\le-\frac{L}{2}+m^*,-\left(x^*+L\right)+m^*\right)\\
&T\left(\frac{L}{2}-m^*\le x^*\le\frac{L}{2},-\left(x^*+m^*\right)+L\right)=T_s\left(\frac{L}{2}-m^*\le x^*\le\frac{L}{2},-\left(x^*+m^*\right)+L\right)\\
&R_k\ \frac{\partial T_s}{\partial n^*}\Big)_{\left(-\frac{L}{2}\le x^*\le-\frac{L}{2}+m^*,-(x^*+L)+m^*\right)}=\frac{\partial T}{\partial n^*}\Big)_{\left(-\frac{L}{2}\le x^*\le-\frac{L}{2}+m^*,-(x^*+L)+m^*\right)}\\
&R_k\ \frac{\partial T_s}{\partial n^*}\Big)_{\left(\frac{L}{2}-m^*\le x^*\le\frac{L}{2},-(x^*+m^*)+L\right)}=\frac{\partial T}{\partial n^*}\Big)_{\left(\frac{L}{2}-m^*\le x^*\le\frac{L}{2},-(x^*+m^*)+L\right)}
\end{aligned}\tag{8}$$

For a general analysis, it is appropriated to express Eqs. (1)–(6) into the non-dimensional forms using dimensionless variables as following:

$$x=\frac{x^*}{L},y=\frac{y^*}{L},m=\frac{m^*}{L},v=\frac{v^*L}{\alpha_{bf}},u=\frac{\mathrm{u}^*L}{\alpha_{bf}},P=\frac{P^*L^2}{\rho_{bf}\alpha_{bf}^2},\theta=\frac{T-T_c}{T_h-T_c},\theta_s=\frac{T_s-T_c}{T_h-T_c},\phi=\frac{C}{\phi_0}\tag{9}$$

substituting Eqs. (9) into Eqs. (1)–(6), the set of Eqs. (10)–(15) is obtained as:

$$\frac{\partial u}{\partial x}+\frac{\partial v}{\partial y}=0\tag{10}$$

$$\frac{1}{R}\left(u\frac{\partial u}{\partial x}+v\frac{\partial u}{\partial y}\right)=-\frac{\partial P}{\partial x}+\frac{\mu_{nf}}{\mu_{bf}}\Pr\left(\frac{\partial^2u}{\partial x^2}+\frac{\partial^2u}{\partial y^2}\right)\tag{11}$$

$$\frac{1}{R}\left(u\frac{\partial v}{\partial x}+v\frac{\partial v}{\partial y}\right)=-\frac{\partial P}{\partial y}+\frac{\mu_{nf}}{\mu_{bf}}\Pr\left(\frac{\partial^2v}{\partial x^2}+\frac{\partial^2v}{\partial y^2}\right)+\frac{NrRa\Pr}{R}(1-\phi)+\frac{Rb\Pr Ra\theta}{R}(1-\phi\phi_0)\tag{12}$$

$$u\frac{\partial\theta}{\partial x}+v\frac{\partial\theta}{\partial y}=\frac{k_{nf}}{k_{bf}}.Rc.\left(\frac{\partial^2\theta}{\partial x^2}+\frac{\partial^2\theta}{\partial x^2}\right)+Nb\left(\frac{\partial\phi}{\partial x}\frac{\partial\theta}{\partial x}+\frac{\partial\phi}{\partial y}\frac{\partial\theta}{\partial y}\right)+Nt\left(\left(\frac{\partial\theta}{\partial x}\right)^2+\left(\frac{\partial\theta}{\partial x}\right)^2\right)\tag{13}$$

$$Le_{bf}\left(u\frac{\partial\phi}{\partial x}+v\frac{\partial\phi}{\partial y}\right)=\frac{\partial^2\phi}{\partial x^2}+\frac{\partial^2\phi}{\partial y^2}+\frac{Nt}{Nb}\left(\frac{\partial^2\theta}{\partial x^2}+\frac{\partial^2\theta}{\partial y^2}\right)\tag{14}$$

$$\frac{\partial^2\theta_s}{\partial x^2}+\frac{\partial^2\theta_s}{\partial y^2}=0\tag{15}$$

where u, v and P are non-dimensional velocity components in horizontal and vertical directions and non-dimensional pressure respectively. Also θ and ϕ are the non-dimensional form of temperature and the volume fraction of nanoparticles respectively. The four parameters *Nr*, *Nb*, *Nt*, and *Le* denote a buoyancy ratio parameter, a Brownian motion parameter, a thermophoresis parameter, and Lewis number respectively. The parameters of Ra, Pr_{bf}, R, Rc, Rb, and R_k are described as:

$$\begin{aligned}
&Nr=\frac{\left(\rho_p-\rho_{bf}\right)\phi_0}{\beta_{bf}\left(T_h-T_c\right)\rho_{nf}},Nb=\frac{\left(\rho C_p\right)_p D_B\phi_0}{\left(\rho C_p\right)_{bf}\alpha_{bf}},Nt=\frac{\left(\rho C_p\right)_p\left(T_h-T_c\right)D_T}{\left(\rho C_p\right)_{bf}\alpha_{bf}T_c},Le_{bf}=\frac{\alpha_{bf}}{D_B},\\
&Ra=\frac{g\beta_{bf}\left(T_h-T_c\right)L^3}{\alpha_{bf}\upsilon_{bf}},\Pr_{bf}=\frac{\upsilon_{bf}}{\alpha_{bf}},R=\frac{\rho_{bf}}{\rho_{nf}},\quad Rc=\frac{(\rho c)_{bf}}{(\rho c)_{nf}},Rb=\frac{\beta_{nf}}{\beta_{bf}},R_k=\frac{k_s}{k_{bf}}.
\end{aligned}\tag{16}$$

The thermal conductivity and the dynamic viscosity of the nanofluid are evaluated as a function of the volume fraction of the nanoparticles in the base fluid as follows [35]:

$$\frac{k_{nf}}{k_{bf}}=(1+Nc\phi_0)\tag{17}$$

$$\frac{\mu_{nf}}{\mu_{bf}}=(1+N\upsilon\phi_0)\tag{18}$$

where Nc and Nv are conductivity parameter and viscosity parameter, respectively. These parameters are generally functions of the size, shape and constructive material of the nanoparticles, the base fluid, and its working temperature. For simplicity, in this study, the values of parameters R, Rc, and Rv are considered constant as they approximately always approach unity for low concentration of nanoparticles. Thus, with mentioned thermal properties of the nanofluid, the resulting equations can be obtained as:

$$u\frac{\partial u}{\partial x}+v\frac{\partial u}{\partial y}=-\frac{\partial P}{\partial x}+(1+Nv\phi_0)\,\mathrm{Pr}\left(\frac{\partial^2 u}{\partial x^2}+\frac{\partial^2 u}{\partial y^2}\right) \tag{19}$$

$$u\frac{\partial v}{\partial x}+v\frac{\partial v}{\partial y}=-\frac{\partial P}{\partial y}+(1+Nv\phi_0)\,\mathrm{Pr}\left(\frac{\partial^2 v}{\partial x^2}+\frac{\partial^2 v}{\partial y^2}\right)+NrRa\,\mathrm{Pr}\,(1-\phi)+(1-\phi\phi_0)\,\mathrm{Pr}\,Ra\theta \tag{20}$$

$$u\frac{\partial \theta}{\partial x}+v\frac{\partial \theta}{\partial y}=(1+Nc\phi_0)\left(\frac{\partial^2 \theta}{\partial x^2}+\frac{\partial^2 \theta}{\partial x^2}\right)+Nb\left(\frac{\partial \phi}{\partial x}\frac{\partial \theta}{\partial x}+\frac{\partial \phi}{\partial y}\frac{\partial \theta}{\partial y}\right)+Nt\left(\left(\frac{\partial \theta}{\partial x}\right)^2+\left(\frac{\partial \theta}{\partial y}\right)^2\right) \tag{21}$$

Three sets of non-dimensional boundary conditions correspond with the velocity, temperature, and the concentration of nanoparticles. (see also [36] and [37]):

$$u=v=0 \text{on the solid walls} \tag{22a}$$

$$\begin{cases} \theta\left(-\frac{1}{2},y\right)=1,\theta\left(\frac{1}{2},y\right)=0, \\ \left.\frac{\partial \theta}{\partial y}\right|_{\left(x,-\frac{1}{2}\right)}=0,\ \left.\frac{\partial \theta}{\partial y}\right|_{\left(x,\frac{1}{2}\right)}=0. \end{cases} \tag{22b}$$

$$\begin{cases} \left.\frac{\partial \phi}{\partial y}\right|_{\left(-\frac{1}{2}+m\le x\le\frac{1}{2},-\frac{1}{2}\right)}=0,\ \left.\frac{\partial \phi}{\partial y}\right|_{\left(-\frac{1}{2}\le x\le\frac{1}{2}-m,\frac{1}{2}\right)}=0, \\ N_b\left.\frac{\partial \phi}{\partial x}\right|_{\left(-\frac{1}{2},-\frac{1}{2}+m\le y\le\frac{1}{2}\right)}+N_t\left.\frac{\partial \theta}{\partial x}\right|_{\left(-\frac{1}{2},-\frac{1}{2}+m\le y\le\frac{1}{2}\right)}=0, \\ N_b\left.\frac{\partial \phi}{\partial x}\right|_{\left(\frac{1}{2},-\frac{1}{2}\le y\le\frac{1}{2}-m\right)}+N_t\left.\frac{\partial \theta}{\partial x}\right|_{\left(\frac{1}{2},-\frac{1}{2}\le y\le\frac{1}{2}-m\right)}=0, \\ N_b\left.\frac{\partial \phi}{\partial n}\right|_{\left(-\frac{1}{2}\le x\le-\frac{1}{2}+m,-(x+1)+m\right)}+N_t\left.\frac{\partial \theta}{\partial n}\right|_{\left(-\frac{1}{2}\le x\le-\frac{1}{2}+m,-(x+1)+m\right)}=0, \\ N_b\left.\frac{\partial \phi}{\partial x}\right|_{\left(\frac{1}{2}-m\le x\le\frac{1}{2},-(x+m)+1\right)}+N_t\left.\frac{\partial \theta}{\partial x}\right|_{\left(\frac{1}{2}-m\le x\le\frac{1}{2},-(x+m)+1\right)}=0. \end{cases} \tag{22c}$$

and the non-dimensional boundary conditions on the interfaces are introduced as:

$$\begin{aligned} &\theta_s\left(-\frac{1}{2}\le x\le-\frac{1}{2}+m,-(x+1)+m\right)=\theta\left(-\frac{1}{2}\le x\le-\frac{1}{2}+m,-(x+1)+m\right) \\ &\theta_s\left(\frac{1}{2}-m\le x\le\frac{1}{2},-(x+m)+1\right)=\theta\left(\frac{1}{2}-m\le x\le\frac{1}{2},-(x+m)+1\right) \\ &R_k\left.\frac{\partial \theta_s}{\partial n}\right)_{\left(-\frac{1}{2}\le x\le-\frac{1}{2}+m,-(x+1)+m\right)}=\left.\frac{\partial \theta}{\partial n}\right)_{\left(-\frac{1}{2}\le x\le-\frac{1}{2}+m,-(x+1)+m\right)} \\ &R_k\left.\frac{\partial \theta_s}{\partial n}\right)_{\left(\frac{1}{2}-m\le x\le\frac{1}{2},-(x+m)+1\right)}=\left.\frac{\partial \theta}{\partial n}\right)_{\left(\frac{1}{2}-m\le x\le\frac{1}{2},-(x+m)+1\right)} \end{aligned} \tag{23}$$

In most studies corresponding to the cavities, the local Nusselt number on the left wall is adapted to analyze the overall rate of heat transfer:

$$Nu_x=-\left((1+Nc\phi_0)\left(\frac{\partial \theta}{\partial x}\right)_{x=-\frac{1}{2}}+R_k\left(\frac{\partial \theta_s}{\partial x}\right)_{x=-\frac{1}{2}}\right) \tag{24}$$

where n is the normal of the surfaces. In the present study, the top and bottom walls of the enclosure are isolated, and the left and right walls have a constant temperature. Since the heat flow is transferred from the high temperature to the low temperature, it is obvious that the mentioned quantities are being corresponded to the left and right walls.

In addition, the average Nusselt number on the left wall of the enclosure is defined as:

$$Nu_{avg}=-\left\{R_k\int_{-\frac{1}{2}}^{m}\frac{\partial \theta_s}{\partial x}dy+(1+Nc\phi_0)\int_{m}^{\frac{1}{2}}\frac{\partial \theta}{\partial x}dy\right\} \tag{25}$$

The non-dimensional form of the heat function for the nanofluid and the solid walls are respectively defined as [6]:

$$\frac{\partial^2 h}{\partial x^2}+\frac{\partial^2 h}{\partial y^2}+\frac{\partial}{\partial x}(\theta v)-\frac{\partial}{\partial y}(\theta u)=0 \tag{26}$$

and,

$$\frac{\partial^2 h}{\partial x^2}+\frac{\partial^2 h}{\partial y^2}=0 \tag{27}$$

The boundary conditions on the left and right walls can be obtained by integrating over the Eqs. (1), (2), (5), and (6).
On the bottom wall:

$$h(-\frac{1}{2}\le x\le\frac{1}{2},-\frac{1}{2})=0 \tag{28}$$

On the left wall:

$$h(-\frac{1}{2},-\frac{1}{2}\le y\le m)=-R_k\int_{-\frac{1}{2}}^{m}\frac{\partial\theta_s}{\partial x}dy \text{ and } h(-\frac{1}{2},m\le y\le\frac{1}{2})=-(1+Nc\phi_0)\int_{m}^{\frac{1}{2}}\frac{\partial\theta}{\partial x}dy \tag{29}$$

On the right wall:

$$h(\frac{1}{2},-\frac{1}{2}\le y\le m)=-(1+Nc\phi_0)\int_{-\frac{1}{2}}^{m}\frac{\partial\theta}{\partial x}dy \text{ and } h(\frac{1}{2},m\le y\le\frac{1}{2})=-R_k\int_{m}^{\frac{1}{2}}\frac{\partial\theta_s}{\partial x}dy \tag{30}$$

On the top wall:

$$h(-\frac{1}{2}\le x\le\frac{1}{2},\frac{1}{2})=-\left\{(1+Nc\phi_0)\int_{-\frac{1}{2}}^{m}\frac{\partial\theta}{\partial x}dy+R_k\int_{m}^{\frac{1}{2}}\frac{\partial\theta_s}{\partial x}dy\right\}=Nu_{avg} \tag{31}$$

where h is the dimensional heat function as $h=h^*/kbf(T_h-T_c)$.

3. Numerical method

To solve the coupled, non-linear and non-dimensional governing Eqs. (14), (15), (19)–(21), (26) and (27) along with the boundary conditions applied (22), (23), (28)–(31), the Galerkin finite element method is employed. The finite element method can be seen in details in [38]. To solve the discussed equations, the penalty finite element method is taken into consideration in which the pressure term in the momentum equations can be eliminated by a penalty parameter defined as follows [39]:

$$P=-\gamma\left(\frac{\partial u}{\partial x}+\frac{\partial v}{\partial y}\right) \tag{32}$$

The mass conservation equation is automatically satisfied for large amounts of γ. Substituting this penalty parameter for pressure term in momentum equations gives the following:

$$u\frac{\partial u}{\partial x}+v\frac{\partial u}{\partial y}=\gamma\frac{\partial}{\partial x}\left(\frac{\partial u}{\partial x}+\frac{\partial v}{\partial y}\right)+(1+Nv\phi_0)\,\mathrm{Pr}\left(\frac{\partial^2 u}{\partial x^2}+\frac{\partial^2 u}{\partial y^2}\right) \tag{33}$$

$$u\frac{\partial v}{\partial x}+v\frac{\partial v}{\partial y}=\gamma\frac{\partial}{\partial y}\left(\frac{\partial u}{\partial x}+\frac{\partial v}{\partial y}\right)+(1+Nv\phi_0)\,\mathrm{Pr}\left(\frac{\partial^2 v}{\partial x^2}+\frac{\partial^2 v}{\partial y^2}\right)+NrRa\,\mathrm{Pr}\,(1-\phi)+(1-\phi\phi_0)\,\mathrm{Pr}\,Ra\theta \tag{34}$$

Using basis set $\xi_k|_{k=1}^{N}$ to expand the existing variables, namely velocity components in x and y directions, temperature, the concentration of the nanoparticles and the heat lines for $0\le x,y\le 1$ as

$$u\approx\sum_{k=1}^{N}u_k\xi_k(x,y)\,,\quad v\approx\sum_{k=1}^{N}v_k\xi_k(x,y)\,,\quad\theta\approx\sum_{k=1}^{N}\theta_k\xi_k(x,y)\,,\phi\approx\sum_{k=1}^{N}\phi_k\xi_k(x,y) \tag{35}$$

and $h\approx\sum_{k=1}^{N}h_k\xi_k(x,y)$, the Galerkin finite element method results in the following seven residual equations for the mentioned Eqs. (14), (15), (19)–(21), (26), and (27) at the internal domain nodes:

$$\begin{aligned}R_i^1=&\sum_{k=1}^{N}u_k\int_\Omega\left[\left(\sum_{k=1}^{N}u_k\xi_k\right)\frac{\partial\xi_k}{\partial x}+\left(\sum_{k=1}^{N}v_k\xi_k\right)\frac{\partial\xi_k}{\partial y}\right]\xi_i dxdy+\gamma\sum_{k=1}^{N}u_k\int_\Omega\frac{\partial\xi_i}{\partial x}\frac{\partial\xi_k}{\partial x}dxdy\\&+\gamma\sum_{k=1}^{N}v_k\int_\Omega\frac{\partial\xi_i}{\partial x}\frac{\partial\xi_k}{\partial y}dxdy+(1+Nv\phi_0)\,\mathrm{Pr}\sum_{k=1}^{N}u_k\int_\Omega\left[\frac{\partial\xi_i}{\partial x}\frac{\partial\xi_k}{\partial x}+\frac{\partial\xi_i}{\partial y}\frac{\partial\xi_k}{\partial y}\right]dxdy\end{aligned} \tag{36}$$

$$R_i^2 = \sum_{k=1}^{N} v_k \int_\Omega \left[\left(\sum_{k=1}^{N} u_k \xi_k \right) \frac{\partial \xi_k}{\partial x} + \left(\sum_{k=1}^{N} v_k \xi_k \right) \frac{\partial \xi_k}{\partial y} \right] \xi_i dxdy + \gamma \left[\sum_{k=1}^{N} u_k \int_\Omega \frac{\partial \xi_i}{\partial y} \frac{\partial \xi_k}{\partial x} + \sum_{k=1}^{N} v_k \int_\Omega \frac{\partial \xi_i}{\partial y} \frac{\partial \xi_k}{\partial y} \right] dxdy +$$
$$(1 + Nv\phi_0) \Pr \sum_{k=1}^{N} v_k \int_\Omega \left[\frac{\partial \xi_i}{\partial x} \frac{\partial \xi_k}{\partial x} + \frac{\partial \xi_i}{\partial y} \frac{\partial \xi_k}{\partial y} \right] dxdy + NrRa \Pr \left(1 - \int_\Omega \sum_{k=1}^{N} \phi_k \xi_k (x, y) \right) +$$
$$\left(1 - \phi_0 \int_\Omega \sum_{k=1}^{N} \phi_k \xi_k (x, y) \right) Ra \Pr \int_\Omega \sum_{k=1}^{N} \theta_k \xi_k (x, y) \tag{37}$$

$$R_i^3 = \sum_{k=1}^{N} \theta_k \int_\Omega \left[\left(\sum_{k=1}^{N} u_k \xi_k \right) \frac{\partial \xi_k}{\partial x} + \left(\sum_{k=1}^{N} v_k \xi_k \right) \frac{\partial \xi_k}{\partial y} \right] \xi_i dxdy + (1 + Nc\phi_0) \sum_{k=1}^{N} \theta_k \int_\Omega \left[\frac{\partial \xi_i}{\partial x} \frac{\partial \xi_k}{\partial x} + \frac{\partial \xi_i}{\partial y} \frac{\partial \xi_k}{\partial y} \right] dxdy$$
$$+ N_b \left[\left(\sum_{k=1}^{N} \phi_k \int_\Omega \frac{\partial \xi_k}{\partial x} \xi_i dxdy \right) \left(\sum_{k=1}^{N} \theta_k \int_\Omega \frac{\partial \xi_k}{\partial x} \xi_i dxdy \right) + \left(\sum_{k=1}^{N} \phi_k \int_\Omega \frac{\partial \xi_k}{\partial y} \xi_i dxdy \right) \left(\sum_{k=1}^{N} \theta_k \int_\Omega \frac{\partial \xi_k}{\partial y} \xi_i dxdy \right) \right] +$$
$$N_t \left[\left(\sum_{k=1}^{N} \theta_k \int_\Omega \frac{\partial \xi_k}{\partial x} \xi_i dxdy \right)^2 + \left(\sum_{k=1}^{N} \theta_k \int_\Omega \frac{\partial \xi_k}{\partial y} \xi_i dxdy \right)^2 \right] \tag{38}$$

$$R_i^4 = \sum_{k=1}^{N} \phi_k \int_\Omega \left[\left(\sum_{k=1}^{N} u_k \xi_k (x, y) \right) \frac{\partial \xi_k}{\partial x} + \left(\sum_{k=1}^{N} v_k \xi_k (x, y) \right) \frac{\partial \xi_k}{\partial y} \right] \xi_i dxdy +$$
$$\sum_{k=1}^{N} \phi_k \int_\Omega \left[\frac{\partial \xi_i}{\partial x} \frac{\partial \xi_k}{\partial x} + \frac{\partial \xi_i}{\partial y} \frac{\partial \xi_k}{\partial y} \right] dxdy + \frac{N_t}{N_b} \sum_{k=1}^{N} \theta_k \int_\Omega \left[\frac{\partial \xi_i}{\partial x} \frac{\partial \xi_k}{\partial x} + \frac{\partial \xi_i}{\partial y} \frac{\partial \xi_k}{\partial y} \right] dxdy \tag{39}$$

$$R_i^5 = R_k \sum_{k=1}^{N} \theta_{s,k} \int_\Omega \left[\frac{\partial \xi_i}{\partial x} \frac{\xi_k}{\partial x} + \frac{\partial \xi_i}{\partial y} \frac{\xi_k}{\partial y} \right] dxdy \tag{40}$$

$$R_i^6 = \sum_{k=1}^{N} h_k \int_\Omega \left[\frac{\partial \xi_i}{\partial x} \frac{\xi_k}{\partial x} + \frac{\partial \xi_i}{\partial y} \frac{\xi_k}{\partial y} \right] dxdy + \left(\sum_{k=1}^{N} \theta_k \int_\Omega \frac{\xi_k}{\partial x} \xi_i dxdy \right) \left(\sum_{k=1}^{N} v_k \int_\Omega \frac{\xi_k}{\partial x} \xi_i dxdy \right) -$$
$$\left(\sum_{k=1}^{N} \theta_k \int_\Omega \frac{\xi_k}{\partial y} \xi_i dxdy \right) \left(\sum_{k=1}^{N} u_k \int_\Omega \frac{\xi_k}{\partial y} \xi_i dxdy \right) \tag{41}$$

$$R_i^7 = \frac{1}{R_k} \sum_{k=1}^{N} h_k \int_\Omega \left[\frac{\partial \xi_i}{\partial x} \frac{\xi_k}{\partial x} + \frac{\partial \xi_i}{\partial y} \frac{\xi_k}{\partial y} \right] dxdy \tag{42}$$

The iterative process is stopped when the convergence criterion $\sqrt{\sum (R_i^j)^2} \leq 10^{-7} 1 \leq j \leq 7$ is reached. A constraint, overall integration of nanoparticles concentration over the domain of solution shall remain unity, is added to keep the concentration of nanoparticles constant.

3.1. Grid check

Various grid sizes were utilized to ensure that the results are independent of the grid size. Here, the mean Nusselt number is used for comparison. Table 1 illustrates the average Nusselt number for two values of nanoparticles concentration, namely 0 and 2%, and for five different grid sizes. It is evident that the grid with 31626 elements can provide acceptable accuracy. Thus, the results of the present study are carried out using the mentioned grid.

3.2. Validation of computation

To check the solution validity, results of the current study has been compared with some of the relevant published articles. For the first investigation, the conjugate heat transfer in a partitioned enclosure adopted by Costa [6] is considered. Costa [6] studied the natural convective heat transfer of a pure fluid (C = 0%) in a partitioned enclosure. Assuming $\phi_0 = 0\%$ (pure fluid) and a different formation of solid walls, the present study shifted to the study of Costa [6]. In this case, the contour of the isotherm is compared with those shown in the work of Costa [3] for $Ra = 10^{+6}$, $Pr = 0.71$ (air) and $R_k = 10$. The results are depicted in Fig. 2. For the second investigation, considering the enclosure without any partition,

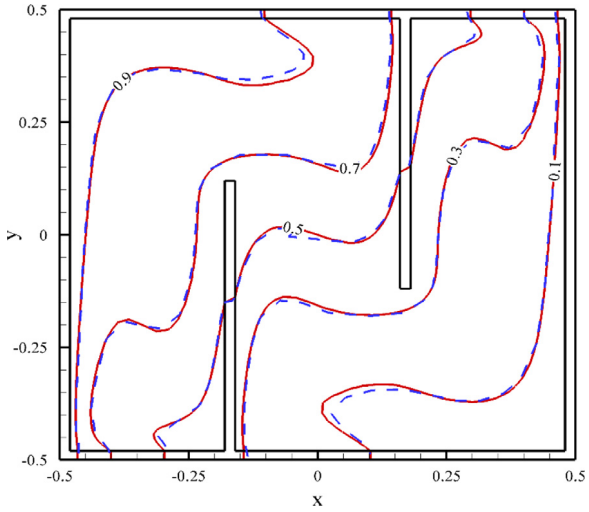

Fig. 2. Comparison of the isotherms of the current study (red lines) and those provided by Costa [6] (dashed blue lines).

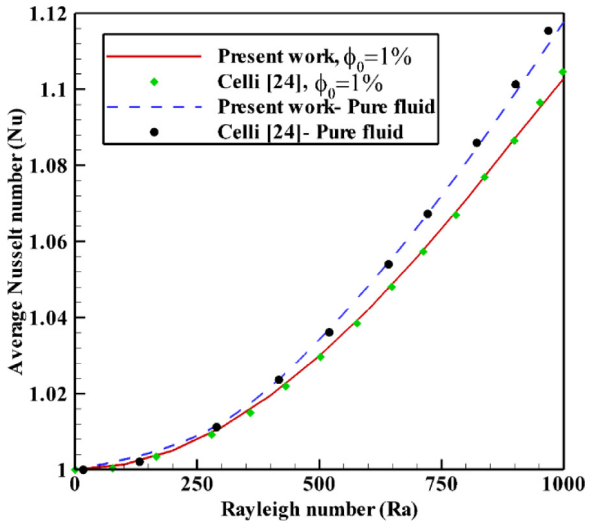

Fig. 3. Comparison between the current study and results of Celli [37] in the absence of the partitions.

Table 1
Grid independency test (Pr = 7, Ra = 10^4, R_k = 500, Nc = Nv = 7, Nb = 1×10^{-6}, Nt = 5×10^{-7}, Nr = 10, Le_{bf} = 6000 and m = 0.25).

	Nu_{Avg}	
Grid size	$\phi_0 = 0\%$	$\phi_0 = 2\%$
6604	2.6414	2.7428
14558	2.6403	2.7418
22818	2.6402	2.7417
31626	2.6398	2.7413
40440	2.6399	2.7414

the average Nusselt number of Water–Al_2O_3 is compared with those reported by Celli [37]. In the study of Celli [37], a side-heated two-dimensional square cavity filled with a nanofluid using non-homogeneous Buongiorno model was taken into consideration. In the study of Celli [37], a different model for thermal conductivity and dynamic viscosity was utilized. In the present study, the values of the Nc and Nv are considered to be equal. Fig. 3 depicts the comparison between the present results and the results reported by Celli [37] for the case study of water–Al_2O_3 nanofluid when the nanofluid

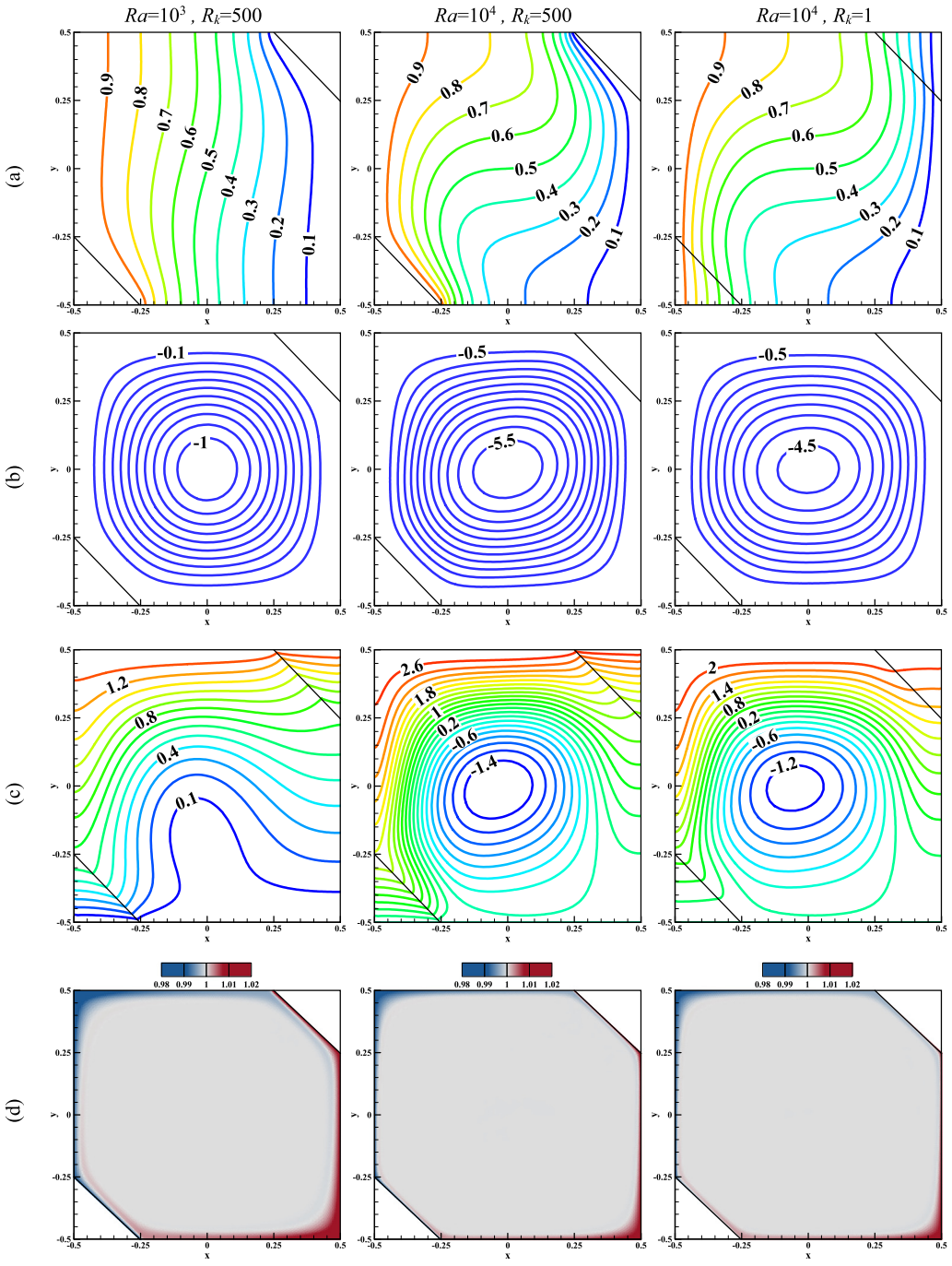

Fig. 4. Effect of the Rayleigh number and thermal conductivity ratio on the (a) contour of isotherms, (b) streamlines, (c) heatlines and (d) surface of nanoparticles concentration (Nc = Nv = 7, Nb = 2Nt = 10^{-6}, m = 0.25).

contains nanoparticles sized 10 *nm* and concentration, $\phi_0 = 1\%$. According to Figs. 2 and 3, an excellent agreement between the results of the present work and Celli [37] and Costa [6] can be found.

4. Results and discussion

Results of the current study are presented in two separate parts. Impact of the parameters and non-dimensional numbers on the rate of heat and mass transfer is investigated in the first part, while the second part is dedicated to the

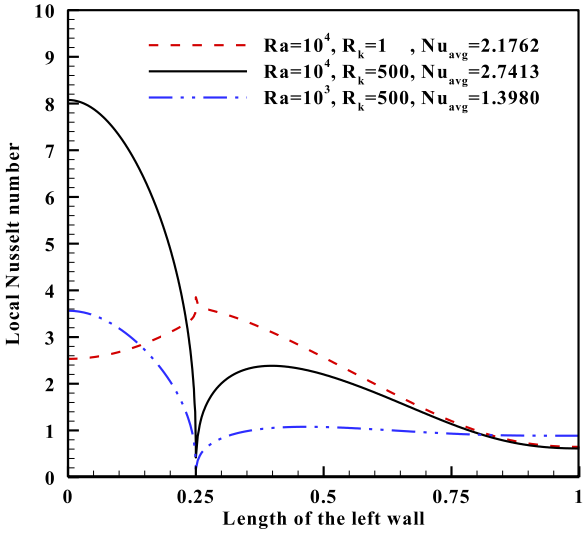

Fig. 5. Effect of the thermal conductivity ratio parameter (R_k) and the Rayleigh number (Ra) on the Local Nusselt number on the left wall (Nc = Nv = 7, Nb = 2Nt = 10^{-6}, m = 0.25).

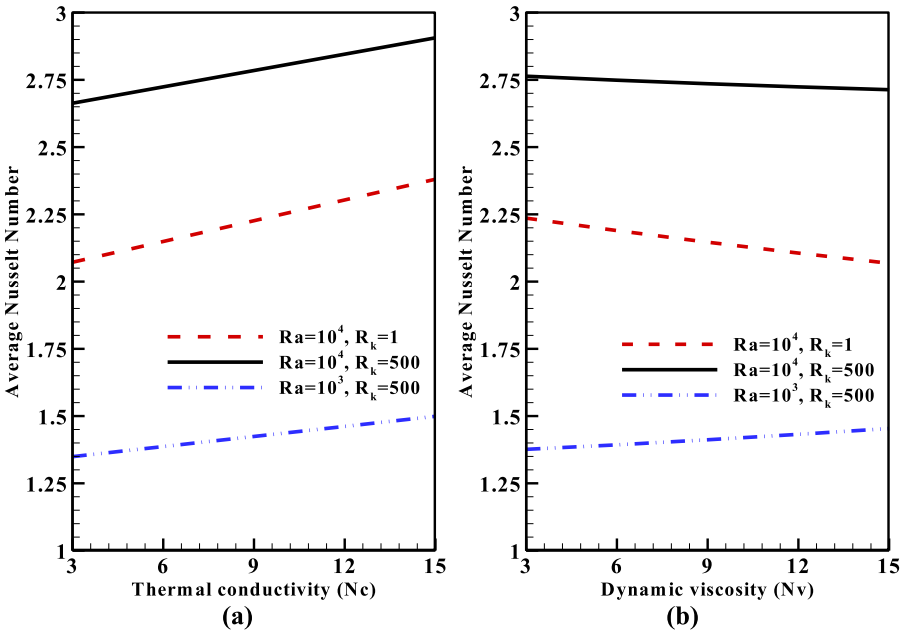

Fig. 6. Impact of (a) Nc (Nv = 7) and (b) Nv (Nc = 7) on the average Nusselt number for different values of the Ra and R_k (Nb = 2Nt = 10^{-6}, m = 0.25).

effect of geometrical parameters on the heat and mass transfer. Influence of parameters such as the Rayleigh number ($10^3 \leq Ra \leq 10^4$), thermal conductivity ratio of solid walls to the fluid ($1 \leq R_k \leq 500$), thermal conductivity parameter ($3 \leq Nc \leq 15$), thermal viscosity parameter ($3 \leq Nv \leq 15$), Brownian motion parameter ($5\times10^{-7} \leq N_b \leq 5\times10^{-6}$), Thermophoresis parameter ($10^{-7} \leq N_b \leq 10^{-6}$), thickness of the triangular walls ($0.0 \leq m \leq 0.75$) and position of the wall is studied. Other parameters such as the Prandtl and Lewis numbers, initial value of nanoparticles concentration and the buoyancy ratio of nanoparticles are kept constant in this study at 7, 6×10^3, 0.02 and 10, respectively.

4.1. Parametric discussion

Effects of the discussed parameters on the rate of heat transfer is studied in this section. The Rayleigh number and thermal conductivity ratio (R_k) are measures of the natural convection and conduction heat transfer and thus are used

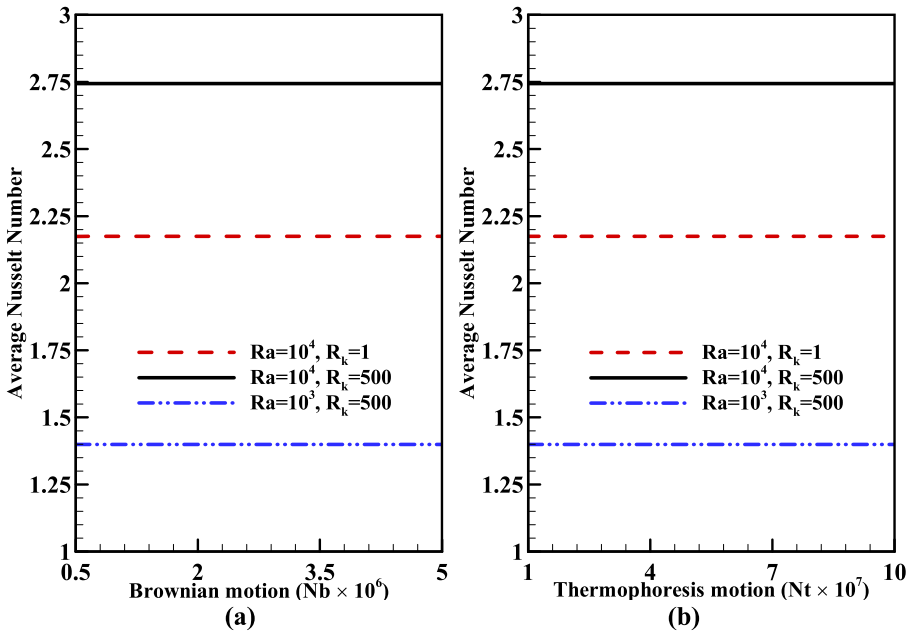

Fig. 7. Impact of (a) Nb ($Nt = 5\times10^{-7}$) and (b) Nt ($Nb = 10^{-6}$) on the mean Nu for different values of the Ra and R_k ($Nc = Nv = 7$, $m = 0.25$).

in this study for comparison. Fig. 4 depicts the effects of mentioned parameters on the isothermal lines (the first row), the streamlines (the second row), the heatlines (the third row) and the distribution of the nanoparticles (the last row) in the cavity. As it is obvious from the first and the second columns, reducing the Ra decreases the deviation of the isothermal lines indicating a reduction in the rate of heat transfer. Moreover, when the conductivity ratio decreases, the isothermal lines pass through the solid triangular walls. As the crowdedness of the isothermal line indicates the higher rate of heat transfer, decreasing the R_k reduces the overall rate of heat transfer. As expected, the reduction of the Ra leads to a drastic reduction on the values of streamlines. Moreover, increasing R_k improves the strength of the flow field. Heatlines are almost horizontal for low Rayleigh numbers, indicating the dominance of the conduction heat transfer. Moreover, the patterns of heatlines deviate from the triangular walls when the R_k reduces, which shows that the lower portion of the heat is transferred from triangular walls. The boundary layers thickness of the nanoparticles along the hot and cold walls on the fourth-row increase as the Rayleigh number decreases results in a reduction in the concentration gradient of the nanoparticles. The decrease in the thermal conductivity ratio leads to the slight increase of the nanoparticles' concentration along triangular walls.

Fig. 5 depicts the effects of the Ra and R_k on the rate of heat transfer. For this purpose, the hot wall is taken into consideration to calculate the values of the local Nu. As expected, decreasing the Ra reduces the values of the local Nusselt number. Lowering the thermal conductivity ratio results in a drastic effect on the local values of the Nu. For low values of the R_k, the triangular walls act as a resistance to heat transfer, and because of that, the local values of the Nu increase ($-0.5 \leq y \leq -0.25$) along the wall. This can be explained by the fact that due to a decrease in the thickness of the wall, the overall heat resistance in solid triangular wall diminishes. Due to the reduction of the temperature gradient along the hot wall ($y \geq -0.25$), the local Nu of the nanofluid decreases on the left wall. Finally, and as expected, the values of the average Nusselt number increases as the Ra increases or the R_k decreases.

The effects of the thermal conductivity (Nc) and thermal viscosity (Nv) parameters on the average Nusselt number are shown in Fig. 6. The average Nusselt number enhances with the increment of the Nc, as it boosts the heat diffusion. Moreover, the flow strength decreases with the augmentation of the thermal viscosity parameter, results in the decline of the overall rate of heat transfer. Evidently, for low values of the Ra, when the conduction is more dominant than the convection heat transfer, the impact of the Nv on the Nu is negligible.

Impact of Nb and Nt on the mean Nu are depicted in Fig. 7. Obviously, while the thermophoresis effect shifts the nanoparticles from hot areas to the cold regions, the Brownian motion impact generally homogenizes the nanoparticles in the fluid. For the current study, the Nu_{avg} is not sensible to the mentioned parameters.

4.2. Geometrical discussion

The size and position of the triangular walls are also of the influential factors on the rate of heat and mass transfer in enclosures. In this section, various geometries consisting of three different thicknessess ($m = 0.0, 0.25, 0.75$) and locations (normal and reverse positions) of the triangular walls are studied.

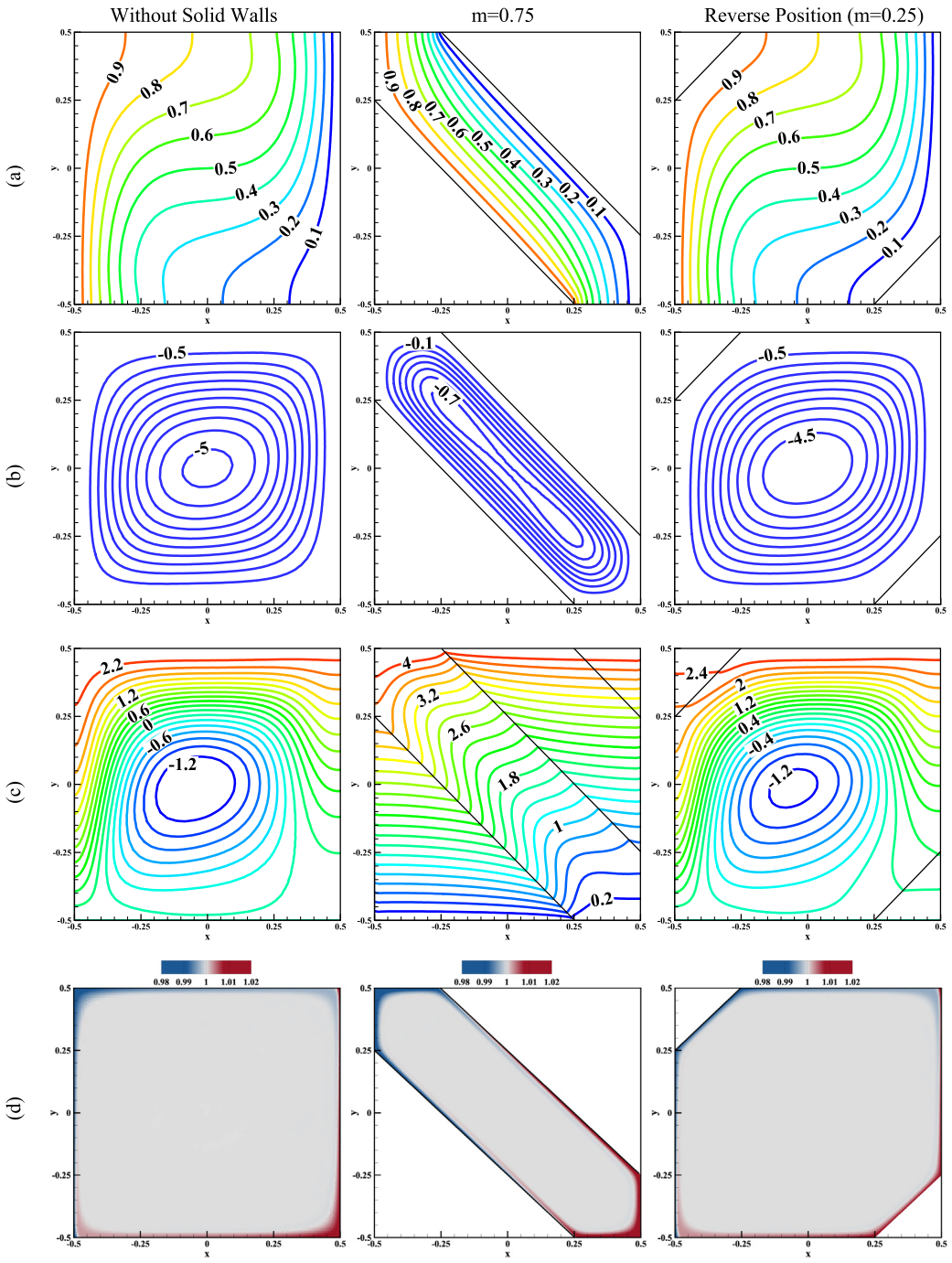

Fig. 8. Effects of size and position of the solid triangular surfaces on the (a) isotherms, (b) streamlines, (c) heatlines and (d) surface of nanoparticles concentration ($Ra = 10^4$, $R_k = 500$, $Nc = Nv = 7$, $Nb = 2Nt = 10^{-6}$).

Fig. 8 illustrates the effects of mentioned geometrical parameters on the patterns of the isotherms (the first row), the streamlines (the second row), the heatlines (the third row) and the concentration of the nanoparticles (the last row). The size of the solid walls shown to have a drastic impact on the flow and thermal fields of the nanofluid as the isotherms and streamlines are formed parallel to the inclined surfaces. The isotherms move slightly toward the hot and cold walls when they are reversely positioned, indicating an overall decrease in the rate of heat transfer (compare with Fig. 4-a). The flow and thermal fields are highly affected by the presence and the thickness of the triangular walls. Comparing with the normal position of the triangular walls, while the heat is mainly transferred through the thin walls when the triangular

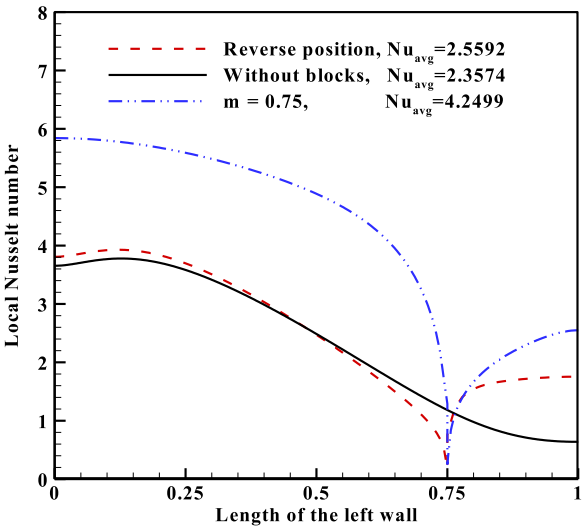

Fig. 9. Evaluation of the effects of three predefined situations on the local Nusselt number (Ra = 10^4, R_k = 500, Nc = Nv = 7, Nb = 2Nt = 10^{-6}, m = 0.25).

blocks are placed on the reverse position, it is mostly transferred through the solid walls when their thickness increases (m = 0.75). The concentration of the nanoparticles along the hot and cold walls increases as the area of the solid walls rises. Moreover, a uniform concentration of the nanoparticles can be observed when the triangular walls are placed on the reverse position.

Fig. 9 compares the effect of the geometrical factors on the local Nusselt number over the hot wall. The temperature difference between the hot wall and the fluid in the upward direction of the flow reduces, resulting in a decrease of the local values of the Nusselt number. The value of the local Nu approaches to about zero on the corner of the triangular wall on the hot wall, specifying the dominant of the conduction heat transfer to the convection mechanism. The total heat transfer decreases when the triangular walls are placed in the reverse position (compare with Fig. 5). Increasing thickness of the triangular walls enhances the local and overall Nusselt number. Moreover, the overall heat transfer boosts in the presence of the triangular walls as it intensifies the rate of heat conduction in the corner of the cavity.

5. Conclusions

In the present paper, the conjugate natural convection heat transfer of a nanofluid in a square enclosure with two solid triangular walls was studied numerically. The left and right walls of the cavity are held at isothermal hot and cold temperatures, T_h and T_c, respectively and the bottom and top are insulated. The Buongiorno model was employed to draw the effects of the thermophoresis and Brownian motions. The outcomes of the study, including streamlines, isotherms, heatlines, and nanoparticles concentration, were depicted and studied. Moreover, the local and mean Nusselt numbers over the entire left hot wall was defined. The influence of varying parameters as well as geometrical factors were studied. Finally, the following conclusions may be drawn:

1. The thermal conductivity ratio affects the patterns of the streamlines, isothermal lines, heatlines and the concentration of the nanoparticles. Decreasing the R_k reduces the overall rate of heat transfer and the strength of the flow field. The nanoparticles' concentration along triangular walls slightly increases as the thermal conductivity ratio decreases.
2. The average Nusselt number enhances with the increment of the thermal conductivity parameter. The flow strength decreases with the augmentation of the thermal viscosity parameter.
3. The thickness and the position of the solid triangular walls influence the flow and thermal fields of the nanofluid drastically. While increasing the thickness of the walls boosts the rate of heat transfer, placing the triangular walls on the reverse position reduces the average Nusselt number. Moreover, the concentration of the nanoparticles along the hot and cold walls increases as the thickness of the solid walls rises.

References

[1] A. Baïri, E. Zarco-Pernia, J.-M.G. De María, A review on natural convection in enclosures for engineering applications. The particular case of the parallelogrammic diode cavity, Appl. Therm. Eng. 63 (2014) 304–322.
[2] A. Bejan, Convection Heat Transfer, John Wiley & Sons, 2013.

[3] A. Ben-Nakhi, A.J. Chamkha, Conjugate natural convection in a square enclosure with inclined thin fin of arbitrary length, Int. J. Therm. Sci. 46 (2007) 467–478.
[4] Y. Varol, H.F. Oztop, A. Varol, Effects of thin fin on natural convection in porous triangular enclosures, Int. J. Therm. Sci. 46 (2007) 1033–1045.
[5] N. Tatsuo, S. Mitsuhiro, K. Yuji, Natural convection heat transfer in enclosures with an off-center partition, Int. J. Heat Mass Transfer 30 (1987) 1756–1758.
[6] V. Costa, Natural convection in partially divided square enclosures: Effects of thermal boundary conditions and thermal conductivity of the partitions, Int. J. Heat Mass Transfer 55 (2012) 7812–7822.
[7] P. Kandaswamy, J. Lee, A.A. Hakeem, S. Saravanan, Effect of baffle–cavity ratios on buoyancy convection in a cavity with mutually orthogonal heated baffles, Int. J. Heat Mass Transfer 51 (2008) 1830–1837.
[8] W. Wu, C.Y. Ching, Laminar natural convection in an air-filled square cavity with partitions on the top wall, in: ASME 2009 Heat Transfer Summer Conference Collocated with the InterPACK09 and 3rd Energy Sustainability Conferences, American Society of Mechanical Engineers, 2009, pp. 399–414.
[9] S.K. Das, S.U. Choi, W. Yu, T. Pradeep, Nanofluids: Science and Technology, John Wiley & Sons, 2007.
[10] H. Tyagi, Radiative and Combustion Properties of Nanoparticle-Laden Liquids, Arizona State University, 2008.
[11] H. Tyagi, P. Phelan, R. Prasher, Predicted efficiency of a low-temperature nanofluid-based direct absorption solar collector, J. Sol. Energy Eng. 131 (2009) 041004.
[12] O. Mahian, A. Kianifar, S.A. Kalogirou, I. Pop, S. Wongwises, A review of the applications of nanofluids in solar energy, Int. J. Heat Mass Transfer 57 (2013) 582–594.
[13] M.A. Ismael, T. Armaghani, A.J. Chamkha, Conjugate heat transfer and entropy generation in a cavity filled with a nanofluid-saturated porous media and heated by a triangular solid, J. Taiwan Inst. Chem. Eng. 59 (2016) 138–151.
[14] S. Parvin, A.J. Chamkha, An analysis on free convection flow, heat transfer and entropy generation in an odd-shaped cavity filled with nanofluid, Int. Commun. Heat Mass Transfer 54 (2014) 8–17.
[15] A.J. Chamkha, M.A. Ismael, Conjugate heat transfer in a porous cavity heated by a triangular thick wall, Numer. Heat Transfer A 63 (2013) 144–158.
[16] A.J. Chamkha, S.H. Hussain, Q.R. Abd-Amer, Mixed convection heat transfer of air inside a square vented cavity with a heated horizontal square cylinder, Numer. Heat Transfer A 59 (2011) 58–79.
[17] N.S. Bondareva, M.A. Sheremet, H.F. Oztop, N. Abu-Hamdeh, Heatline visualization of MHD natural convection in an inclined wavy open porous cavity filled with a nanofluid with a local heater, Int. J. Heat Mass Transfer 99 (2016) 872–881.
[18] I.V. Miroshnichenko, M.A. Sheremet, H.F. Oztop, K. Al-Salem, MHD natural convection in a partially open trapezoidal cavity filled with a nanofluid, Int. J. Mech. Sci. 119 (2016) 294–302.
[19] M.A. Sheremet, D.S. Cimpean, I. Pop, Free convection in a partially heated wavy porous cavity filled with a nanofluid under the effects of Brownian diffusion and thermophoresis, Appl. Therm. Eng. 113 (2017) 413–418.
[20] M.A. Sheremet, T. Groşan, I. Pop, Steady-state free convection in right-angle porous trapezoidal cavity filled by a nanofluid: Buongiorno's mathematical model, Eur. J. Mech. B/Fluids 53 (2015) 241–250.
[21] N.S. Bondareva, M.A. Sheremet, H.F. Oztop, N. Abu-Hamdeh, Heatline visualization of natural convection in a thick walled open cavity filled with a nanofluid, Int. J. Heat Mass Transfer 109 (2017) 175–186.
[22] N.S. Bondareva, M.A. Sheremet, H.F. Oztop, N. Abu-Hamdeh, Entropy generation due to natural convection of a nanofluid in a partially open triangular cavity, Adv. Powder Technol. 28 (2017) 244–255.
[23] D.S. Bondarenko, M.A. Sheremet, H.F. Oztop, M.E. Ali, Natural convection of Al2O3/H2O nanofluid in a cavity with a heat-generating element. Heatline visualization, Int. J. Heat Mass Transfer 130 (2019) 564–574.
[24] A.I. Alsabery, M.A. Sheremet, A.J. Chamkha, I. Hashim, Impact of nonhomogeneous nanofluid model on transient mixed convection in a double lid-driven wavy cavity involving solid circular cylinder, Int. J. Mech. Sci. 150 (2019) 637–655.
[25] A.I. Alsabery, M.A. Sheremet, A.J. Chamkha, I. Hashim, MHD convective heat transfer in a discretely heated square cavity with conductive inner block using two-phase nanofluid model, Sci. Rep. 8 (2018) 7410.
[26] I. Hashim, A.I. Alsabery, M.A. Sheremet, A.J. Chamkha, Numerical investigation of natural convection of Al2O3-water nanofluid in a wavy cavity with conductive inner block using Buongiorno's two-phase model, Adv. Powder Technol. 30 (2019) 399–414.
[27] A.I. Alsabery, T. Armaghani, A.J. Chamkha, I. Hashim, Conjugate heat transfer of al2o3–water nanofluid in a square cavity heated by a triangular thick wall using Buongiorno's two-phase model, J. Therm. Anal. Calorim. 135 (2019) 161–176.
[28] H.F. Oztop, E. Abu-Nada, Numerical study of natural convection in partially heated rectangular enclosures filled with nanofluids, Int. J. Heat Fluid Flow 29 (2008) 1326–1336.
[29] E. Abu-Nada, Z. Masoud, H.F. Oztop, A. Campo, Effect of nanofluid variable properties on natural convection in enclosures, Int. J. Therm. Sci. 49 (2010) 479–491.
[30] E. Abu-Nada, A.J. Chamkha, Mixed convection flow in a lid-driven inclined square enclosure filled with a nanofluid, Eur. J. Mech. B Fluids 29 (2010) 472–482.
[31] M. Sheikholeslami, M. Gorji-Bandpy, S. Seyyedi, D. Ganji, H.B. Rokni, S. Soleimani, Application of LBM in simulation of natural convection in a nanofluid filled square cavity with curve boundaries, Powder Technol. 247 (2013) 87–94.
[32] J. Buongiorno, Convective transport in nanofluids, J. Heat Transfer 128 (2006) 240–250.
[33] A. Zaraki, M. Ghalambaz, A.J. Chamkha, M. Ghalambaz, D. De Rossi, Theoretical analysis of natural convection boundary layer heat and mass transfer of nanofluids: effects of size, shape and type of nanoparticles, type of base fluid and working temperature, Adv. Powder Technol. 26 (2015) 935–946.
[34] A.J. Chamkha, M.A. Ismael, Conjugate heat transfer in a porous cavity filled with nanofluids and heated by a triangular thick wall, Int. J. Therm. Sci. 67 (2013) 135–151.
[35] M. Sabour, M. Ghalambaz, A. Chamkha, Natural convection of nanofluids in a cavity: criteria for enhancement of nanofluids, Internat. J. Numer. Methods Heat Fluid Flow 27 (2017) 1504–1534.
[36] M.A. Sheremet, I. Pop, Conjugate natural convection in a square porous cavity filled by a nanofluid using Buongiorno's mathematical model, Int. J. Heat Mass Transfer 79 (2014) 137–145.
[37] M. Celli, Non-homogeneous model for a side heated square cavity filled with a nanofluid, Int. J. Heat Fluid Flow 44 (2013) 327–335.
[38] J.N. Reddy, An Introduction to the Finite Element Method, New York, 1993.
[39] T. Basak, S. Roy, A. Balakrishnan, Effects of thermal boundary conditions on natural convection flows within a square cavity, Int. J. Heat Mass Transfer 49 (2006) 4525–4535.